Published in final edited form as:
*Int J Radiat Oncol Biol Phys*. 2013 July 15; 86(4): 762–768. doi:10.1016/j.ijrobp.2013.03.007.

# Automatic prostate tracking and motion assessment in volumetric modulated arc therapy with an electronic portal imaging device

**Juan Diego Azcona, Ph.D.**[1,2], **Ruijiang Li, Ph.D.**[1], **Edward Mok, M.Sc.**[1], **Steven Hancock, M.D.**[1], and **Lei Xing, Ph.D.**[1]

[1]Department of Radiation Oncology, Stanford University, Stanford, California 94305

[2]Department of Oncology, Division of Radiation Physics, Clínica Universidad de Navarra, 31080 Pamplona, Navarra, Spain

## Abstract

**Purpose—**To assess the prostate intrafraction motion in volumetric modulated arc therapy treatments using cine megavoltage (MV) images acquired with the electronic portal imaging device (EPID).

**Materials and methods—**Ten prostate cancer patients were treated with volumetric modulated radiation therapy (VMAT), using a Varian TrueBeam (Varian Medical Systems, Palo Alto, CA) linear accelerator (linac) equipped with EPID for acquiring cine MV images during treatment. Cine MV images acquisition was scheduled for single or multiple treatment fractions (between 1 and 8). A novel automatic fiducial detection algorithm that can handle irregular multileaf collimator (MLC) apertures, field edges, fast leaf and gantry movement, and MV image noise and artifacts in patient anatomy was used. All sets of images (~25,000 images in total) were analyzed to measure the positioning accuracy of implanted fiducial markers and assess the prostate movement.

**Results—**Prostate motion can vary greatly in magnitude among different patients. Different motion patterns were identified showing its unpredictability. The mean displacement and standard deviation of the intrafraction motion was generally less than 2.0 ± 2.0 mm in each of the spatial directions. In certain patients, however, the percentage of the treatment time in which the prostate is displaced more than 5 mm from its planned position in at least one spatial direction was 10% or more. The maximum prostate displacement observed was 13.3 mm.

**Conclusion—**Prostate tracking and motion assessment was performed with MV imaging and an EPID. The amount of prostate motion observed suggests that patients will benefit from its real-time monitoring. MV imaging can provide the basis for real-time prostate tracking using conventional linacs.



Corresponding author: Juan Diego Azcona, Ph. D., Department of Radiation Oncology, Stanford University School of Medicine, 875 Blake Wilbur Drive, Stanford, CA 94305, Phone: 650-724-3226, Fax: 650-498-5008, jdazcona@stanford.edu.

**Conflict of interest disclosure:** None

**Keywords**

image-guided radiation therapy; tumor tracking; MV imaging; VMAT; intrafraction motion; motion management; prostate radiation therapy

## I. INTRODUCTION

Patients affected by prostate cancer can be greatly benefited from the escalation of the prescribed dose that is allowed nowadays by modern radiotherapy techniques such as intensity modulated radiation therapy (IMRT) and volumetric modulated arc therapy (VMAT). However, in order to fully exploit the advantages of these highly conformation techniques, image guidance is necessary to ensure that the beam targeting is accurate enough to provide with full tumor coverage whilst decreasing the tumor margins as well as adequate healthy tissue sparing. Patient reproducibility between different fractions to control interfraction motion of the prostate, as well as movement in a single fraction (intrafraction motion) are issues to be addressed in any image-guided radiation therapy (IGRT) program. Prostate tracking and intrafraction motion assessment has been performed by means of Calypso electromagnetic transponders in real-time (1–4), kilovoltage (kV) and megavoltage (MV) imaging based on fiducial markers, employing daily portal images (5–7), pre- and post- treatment delivery kV and treatment beam MV images (8), cone-beam computed tomography (CBCT) (9), continuous kV imaging (10), x-ray stereoscopic imaging taken periodically during treatment with CyberKnife (11), and real-time tumor-tracking radiotherapy with a dedicated machine (RTRT) (12). Cine magnetic resonance imaging (MRI) images (13), and ultrasound (14) have also been employed.

Using the Calypso system, Langen *et al.* (4) reported that the prostate was displaced more than 3 mm by 13.6% of the time on average (mean tracking time: 10 minute, with standard deviation of 2 min), although this number varied greatly between the patients studied. Similar result (prostate displaced over 3 mm 15.2% of the time in 10 min lasting treatments) was found by Malinowski *et al.* (15). Also according to (4), 10 min after the setup, 25% of the patients showed a prostate displacement > 3 mm, demonstrating that the likelihood of the displacement increases with the elapsed time since the setup. This was also shown by Adamson and Wu (9). Willoughby *et al.* (2) observed motion larger than 10 mm that persisted more than 1 min in 2 patients out of 11, in treatments that lasted 8 min. Using portal images in 427 patients, Kotte *et al.* (5) reported displacements over 3 mm in 28% of the fractions for treatment times between 5–7 min. They also showed that the percentage of time that the prostate can move from its initial position within a single fraction depended on the duration of the treatment. The different types of movements that can occur were described and classified by Kupelian *et al.* (1), studying treatments lasting roughly between 540 and 660 secs. The trajectories they reported showed clearly that prostate continuous motion was unpredictable. In that study, they also reported prostate cumulative displacements of more than 3 mm and at least 30 secs. of duration in 41% of the sessions. These data stressed the importance of a good image guidance strategy to ensure that the tumor is within the predefined margins of treatment when pursuing dose escalation with margin reduction.

The use of continuous cine MV tracking proposed in this paper has several advantages over the previous state-of-the-art. Electromagnetic transponders (1–4) are relatively big as compared to fiducial markers and create artifacts on the magnetic resonance images (MRI), an imaging modality commonly employed for prostate patients follow-up. Portal images and CBCT based tracking techniques (5–9) cannot provide real-time motion information. Fluoroscopic kV imaging (10) entails the delivery of additional imaging dose to the patient.

MV imaging has the fundamental advantage of using the therapeutic beam to image what is actually being irradiated in the patient, avoiding the delivery of additional imaging dose. A combined on demand hybrid kV/MV strategy (16) was also proposed but no clinical study has been performed up to now. Mao *et al.* (17) used MV tracking for a single patient treated with IMRT fields. Since fixed gantry IMRT is not continuous irradiation, the fiducials could move while not being imaged and 3D trajectories could not be reconstructed.

This work describes our clinical implementation of prostate motion tracking and 3D trajectory reconstruction based solely on MV imaging during VMAT treatments. We present measured data of the prostate motion during treatment and analyzed retrospectively using a novel automatic fiducial detection algorithm (18). The technique proposed has the advantage of being readily implementable with the equipment currently available in modern linacs. Since VMAT enables continuous radiation beam, the beam targeting is expected to improve when tracking the tumor during treatment. Furthermore, VMAT treatment times are shorter, which results in less probability of motion.

## II. MATERIAL AND METHODS

### A) Patient selection, positioning, and treatment

Ten patients with locally advanced prostate cancer underwent radiotherapy with curative intent as their treatment option. Fast VMAT radiotherapy treatments were provided with a Varian TrueBeam (Varian Medical Systems, Palo Alto, California) linac. The linac was equipped with electronic portal imaging device (EPID) and could acquire cine MV images during treatment at a rate of ~ 5 frames/sec. and a resolution of 0.392 mm per pixel. The Varian iTools™ software was used to obtain the images in its original resolution for the subsequent analysis.

All of the patients have three fiducial markers implanted in the prostate. The treatment plan consisted in all cases in two volumetric modulated arcs, each one being delivered in about 60 seconds. Four of the patients had weekly cine MV imaging and the remaining had between one and four set of images taken on different days. The patients were positioned with two orthogonal kV portal images followed with a 2D/2D matching of the fiducials with their projection from the planning CT. Couch translation movements to eventually fine adjust the patient positioning were performed according to the matching results.

### B) Automatic fiducial detection and 3D position estimation

An automatic fiducial detection algorithm was developed that detected the fiducial positions in cine MV images acquired with the therapeutic beam (18). It employed a prediction model for the expected fiducial position on an image, based on its previous detections in the same arc during that fraction of treatment. The algorithm used a combined criterion of shape similarity by template matching and image intensity to recognize the fiducial markers as projected in the MV image. A universal template formula was used for fiducial detection in all patients taking into account the fiducial orientation as well as the case in which the fiducials were close to or partially occluded by the leaves. Electronic artifacts in the EPID image when the system was working were effectively removed in order to use the image intensity. The search area was dynamically adapted between subsequent images to track the fiducial motion. The algorithm could successfully detect fiducial markers in >90% of the MV images acquired during patient VMAT treatments (18). The average error in the detection was typically less than 1 mm (18). Figure 1 contains two images with fiducial detection on MV images taken with an EPID on which the fiducials have been detected in VMAT treatments. After the two-dimensional (2D) displacements of the fiducial were measured on a particular image, the three-dimensional (3D) fiducial trajectories were

estimated from all the fiducial 2D positions for the images at previous gantry angles in that arc according to the work of Li *et al.* (19).

### C) Assessment of fiducial detectability and prostate motion

The motion assessment through the whole treatment fraction varied depending upon the number of images in which the fiducials could be detected. Fiducial blockage could hinder the tracking. We first present our data about the complexity of the plans with detectability of each of the fiducials for the two arcs in every patient treatment. For each arc, we stated the percentage of images in which each fiducial was detected, as well as the percentage of images in which at least one fiducial was detected. The detection happened at every time in which the expected position of the fiducial, calculated according to the prediction scheme in our algorithm based on the previous detected positions, lied in open beam.

Prostate motion trajectories based on the fiducial position detection were derived. The mean of the anterior-posterior (AP), lateral (LAT), superior-inferior (SI), and absolute (ABS) lengths of the displacements among all fractions and arcs for each patient was calculated along with their standard deviation ($\sigma$). Since the treatment time was short, it was expected to limit the motion amplitude (6). For the four patients with acquisition of weekly cine MV images, the mean absolute displacement in each fraction was calculated, as well as its standard deviation, as an assessment of the reproducibility of the targeting error between different fractions. Furthermore, we identified several patterns of trajectories examining the data available for the displacements in each fraction and arc. The percentage of the tracked time in which the displacement exceeds 3 and 5 mm for each patient has also been assessed.

## III. RESULTS

Table I presents the data of the detections of the three fiducials according to the algorithm outlined in Section II.B, as well as the percentage of images with at least one fiducial was detected. The detectability of the fiducials depended heavily on the control point configuration of the VMAT fields that could block them. Two situations of largely blocked fiducials can be seen in the counterclockwise (CCW) arcs of patients 3 and 6.

In Table II we present the motion assessed for each one of the patients studied. To summarize, the mean of the absolute value of the displacement is presented in each of the 3D directions, as well as the absolute value of the displacement, with their corresponding standard deviation value ($\sigma$). Based on the 3D trajectories derived from the measured data on the EPID, the fraction of the treatment time in which the fiducials are at a distance larger than 3 mm and 5 mm from their planned positions was calculated and is represented in Table III. The mean displacement and standard deviation of the intrafraction motion was generally less than $2.0 \pm 2.0$ mm in each of the space directions, although when combined to calculate the 3D displacement it was likely to go beyond that value.

The prostate motion depended on each patient and, for each patient it was different between fractions. Figure 2 contains the plot of the mean of the absolute value of the overall displacement (averaged among the 3D estimated value from the whole set of images used for measurement) for each fiducial and fraction, for the four patients with weekly cine MV images. The mean displacement was reproducible for the fractions imaged along the course of the treatment within a standard deviation less than 1 mm, but its value goes above 2 mm in three cases, being all fast treatments (around 2 min in time duration).

Figure 3 presents several distinct prostate motion patterns measured in the patients with the EPID, after removing the bad 2D detections (algorithm localizations that deviate from the ground truth as determined by manual localization by more than half the dimension of the

fiducial as seen on the MV image, that is, ~2 mm). Stable target at baseline (row 1), continuous drift (row 2), transient excursion (row 3), persistent excursions (rows 4 and 5) and combination of drift and excursions were seen. High frequency excursions were also identified in trajectory (row) 2.

Table III presents the estimation the fraction of time for each patient and spatial direction with a displacement larger than 3 and 5 mm. It was found to vary a lot among different patients (from 0.1% to 32.1% for 3 mm displacements and from 0.0% to 24.1% for 5 mm displacements. The beam targeting varied greatly between different patients and the margins needed for ensuring a safe prostate radiotherapy procedure are thus patient dependent.

## IV. DISCUSSION

In this work we assessed prostate intrafraction motion during VMAT treatments using cine MV imaging. The use of the VMAT technique, which is faster than the conventional IMRT, is expected to limit the prostate motion since the likelihood of the displacement of the prostate gland decreases with shorter treatment time (4,9). Different trajectories could be identified for different treatment fractions even for the same patient. For example, trajectories 1 and 2 in Figure 3 correspond to patient 1, and trajectories 3 and 5 to patient 2. Trajectory 5 corresponds to fraction 7 in patient 2 and the large permanent excursion at the end of the track caused the mean and standard deviation to increase, as can be seen in Figure 2. We characterized the mean intrafraction motion for the patients studied, which varied between patients and could be >2 mm, as well as the amount of time in which the displacement was larger than 3 and 5 mm. In some patients, the prostate could move >5 mm in any of the directions for nearly 10% of the tracked time (Table III). These findings emphasize the need of a real-time image guidance strategy to be able to increase the prescribed dose reducing the tumor's margins, thus allowing the dose escalation. These results also indicate that the treatment margins should be patient dependent or individualized in order to maximally benefit from the conformal dose distributions in VMAT.

MV fiducial detection can provide the basis for real-time tumor guidance. In this work we demonstrated its feasibility, using the capabilities already available in current linacs. It is worth to discuss briefly the challenges posed by real-time implementation. First, the time needed for processing each image with the current implementation of our method was ~1 sec, which included template matching search and mask generation. Translating the code to a low level language such C is expected to increase its speed by at least one order of magnitude. Furthermore, the effect of fiducial occlusion by the leaves could be alleviated by encouraging at least one fiducial to be under open beam during the treatment planning process. This work was done by Ma *et al.* (20) in the context of four dimensional (4D) optimization with IMRT fields. An approach in real-time implementation would be to stop the beam delivery when the displacement estimation exceeds a pre-established threshold. Although 2D displacements as measured on the EPID are readily available and could be used for detecting a displacement threshold, the use of 3D estimation displacements is more robust, especially when using continuous tracking. The 3D Bayesian tracking algorithm is effective in estimating dynamic target position (19). Given a cine MV projection image, two position parameters are determined. The only unknown parameter is the target position parallel with the MV beam, which is estimated by combining the information from the current projection (as likelihood) and previous projections (as prior) in a Bayesian framework. Furthermore, the effect of uncertainties in target position along the treatment beam on the final dose distributions is expected to be small. A displacement can be promptly detected and assessed, enabling fast intervention in real-time. The MV information could be complemented with an orthogonal kV image to calculate accurately the 3D position of the fiducials by triangulation and confirm the actual motion (16).

An explanation is needed for the AP displacement for patient 7. He had only two fractions tracked and in one of them he had complex prostate movement (either rotation of deformation) that cannot be compensated by pitching the couch (Figure 1, left, shows the fiducial displacements detected in one MV image). That was the reason for having 24.1% of the time with a displacement over 5 mm in the AP direction. The trajectory during this fraction is showed in Fig. 3, row 4. In this patient the assessed displacement was predominant in the AP direction, with no correlation in the SI direction. A similar explanation can be made for the trajectory shown in Fig. 3, row 5 (patient 2). The fiducial displacements were different among the three directions for most of the track (the image in Fig. 1, right shows the prostate movement).

## V. CONCLUSION

Prostate intrafraction motion assessment based on cine MV imaging during VMAT treatments is feasible. Generally, prostate motion tends to be random without a fixed pattern, which necessitates real-time monitoring of intrafractional prostate motion even for rotational arc therapy with conventional fractionation scheme. Imaging in between arcs may be helpful, but there is no guarantee that the motion will happen only at the end of each arc. Moreover, to document and verify the target position during IMRT or arc therapy delivery, real-time monitoring of prostate position is important and should be an integral part of modern radiation therapy treatment systems. Prostate patients would greatly benefit from a real-time image guidance strategy that allows margin reduction and dose escalation. Automatic fiducial detection using an EPID can provide safe, economic, imaging dose-free, and efficient approach for real-time image guided prostate radiotherapy.

## Acknowledgments

This work was supported by National Institutes of Health grants 1R21 CA153587, 1R01 CA133474 and 1K99 CA166186, and Varian Medical Systems.

## References

1. Kupelian P, Willoughby T, Mahadevan A, et al. Multi-institutional clinical experience with the Calypso system in localization and continuous, real-time monitoring of the prostate gland during external radiotherapy. Int J Radiat Oncol Biol Phys. 2007; 67:1088–1098. [PubMed: 17187940]
2. Willoughby TR, Kupelian P, Pouliot J, et al. Target localization and real-time tracking using the Calypso 4D localization system in patients with localized prostate cancer. Int J Radiat Oncol Biol Phys. 2006; 65:528–534. [PubMed: 16690435]
3. Litzenberg DW, Balter JM, Hadley SW, et al. Influence of intrafraction motion on margins for prostate radiotherapy. Int J Radiat Oncol Biol Phys. 2006; 65(2):548–553. [PubMed: 16545919]
4. Langen KM, Willoughby TR, Meeks SL, et al. Observations on real-time prostate gland motion using electromagnetic tracking. Int J Radiat Oncol Biol Phys. 2008; 71(4):1084–1090. [PubMed: 18280057]
5. Kotte ANTJ, Hofman P, Lagendijk JJW, et al. Intrafraction motion of the prostate during external-beam radiation therapy: Analysis of 427 patients with implanted fiducial markers. Int J Radiat Oncol Biol Phys. 2007; 69(2):419–425. [PubMed: 17513059]
6. Aubry JF, Beaulieu L, Girouard LM, et al. Measurements of intrafraction motion and interfraction and intrafraction rotation of prostate by three-dimensional analysis of daily portal imaging with radiopaque markers. Int J Radiat Oncol Biol Phys. 2004; 60(1):30–39. [PubMed: 15337537]
7. Neverdeen AJ, van der Heide UA, Dehnad H, et al. Measurements and clinical consequences of prostate motion during a radiotherapy fraction. Int J Radiat Oncol Biol Phys. 2002; 53(1):206–214. [PubMed: 12007961]

8. Mutanga TF, de Boer HCJ, Rajan V, et al. Day-to-day reproducibility of prostate intrafraction motion assessed by multiple kV and MV imaging of implanted markers during treatment. Int J Radiat Oncol Biol Phys. 2012; 83(1):400–407. [PubMed: 22019244]
9. Adamson J, Wu Q. Prostate intrafraction motion assessed by simultaneous kilovoltage fluoroscopy at megavoltage delivery I: Clinical observations and pattern analysis. Int J Radiat Oncol Biol Phys. 2010; 78(5):1563–1570. [PubMed: 20579817]
10. Ng JA, Booth JT, Poulsen PR, et al. Kilovoltage intrafraction monitoring for prostate intensity modulated arc therapy: First clinical results. Int J Radiat Oncol Biol Phys. 2012; 84(5):e655–e661. [PubMed: 22975613]
11. Xie Y, Djajaputra D, King CR, et al. Intrafraction motion of prostate in hypofractionated radiation therapy. Int J Radiat Oncol Biol Phys. 2008; 72:236–246. [PubMed: 18722274]
12. Kitamura K, Shirato H, Seppenwolde Y, et al. Three-dimensional intrafractional movement of prostate measured during real-time tumor-tracking radiotherapy in supine and prone treatment positions. Int J Radiat Oncol Biol Phys. 2002; 53(5):1117–1123. [PubMed: 12128110]
13. Ghilezan MJ, Jaffray DA, Siewerdsen JH, et al. Prostate gland motion assessed with cine-magnetic resonance imaging (cine-MRI). Int J Radiat Oncol Biol Phys. 2005; 62(2):406–417. [PubMed: 15890582]
14. Huang E, Dong L, Chandra A, et al. Intrafraction prostate motion during IMRT for prostate cancer. Int J Radiat Oncol Biol Phys. 2002; 53(2):261–268. [PubMed: 12023128]
15. Malinowski KT, Noel C, Roy M, et al. Efficient use of continuous, real-time prostate localization. Phys Med Biol. 2008; 53:499–4970.
16. Liu W, Wiersma RD, Xing L. Optimized hybrid megavoltage-kilovoltage imaging protocol for volumetric prostate arc therapy. Int J Radiat Oncol Biol Phys. 2010; 78(2):595–604. [PubMed: 20472354]
17. Mao W, Hsu A, Riaz N, et al. Image-guided radiotherapy in near real time with intensity-modulated radiotherapy megavoltage treatment beam imaging. Int J Radiat Oncol Biol Phys. 2009; 75(2):603–610. [PubMed: 19735886]
18. Azcona JD, Li R, Mok E, et al. Development and clinical evaluation of automatic fiducial detection for tumor tracking in cine megavoltage images during volumetric modulated arc therapy. Med Phys. In press.
19. Li R, Fahimian BP, Xing L. A Bayesian approach to real-time 3D tumor localization via monoscopic x-ray imaging during treatment delivery. Med Phys. 2011; 38:4205–4214. [PubMed: 21859022]
20. Ma Y, Lee L, Keshet O, et al. Four-dimensional inverse treatment planning with inclusion of implanted fiducials in IMRT segmented fields. Med Phys. 2009; 36(6):2215–2221. [PubMed: 19610310]

## Summary

The amount of prostate motion and its unpredictability and variability among patients requires its real-time monitoring to benefit most patients. We have used a conventional linear accelerator and MV imaging with an EPID to track and assess the prostate motion during VMAT treatments. The proposed strategy successfully demonstrated the potential of MV imaging to monitor prostate motion based on implanted fiducials and could be implemented in real-time.

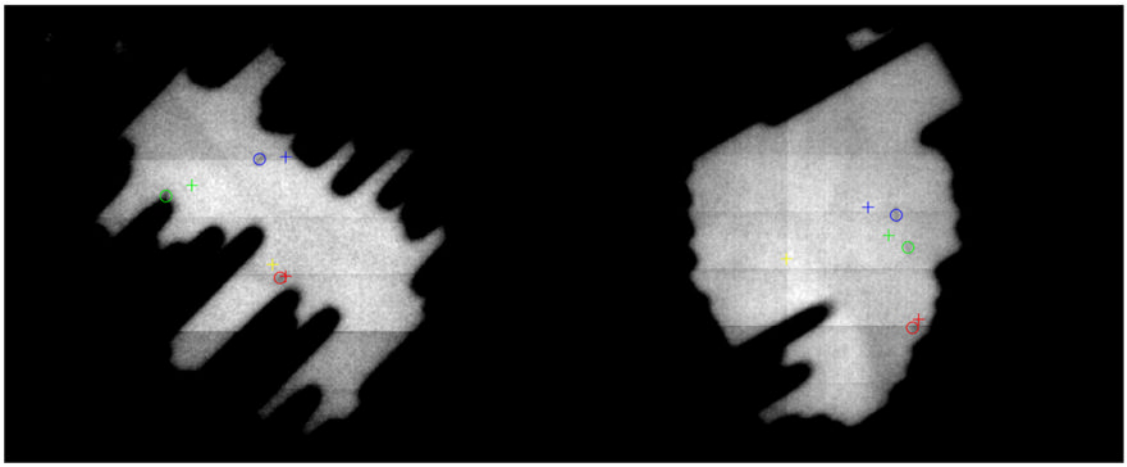

**Figure 1.**
Detection of the three fiducials on EPID MV images. The CT planned positions of the fiducials are depicted by crosses and the localized positions with circles. Left: In this challenging situation in which the fiducials are close to the leaf edges for this leaves configuration, the algorithm is able to successfully detect several mm of displacement detected for fiducials 1 (blue) and 2 (green). Fiducial 3 is displayed in red and the projection of the isocenter is represented by the yellow cross. This patient's motion statistics are summarized in case 7 in the data Tables. The whole motion trajectory is showed in Figure 3, row 4. The gantry angle for this image is 221.6 degrees. Right: This image corresponds to the motion depicted in Fig. 3, row 5 (overall statistics for all fractions in case 2 in the Tables). The gantry angle is 99.9 degrees. A gantry angle of 0 degrees corresponds to an anterior-posterior beam and the gantry angle increases in the clockwise direction.

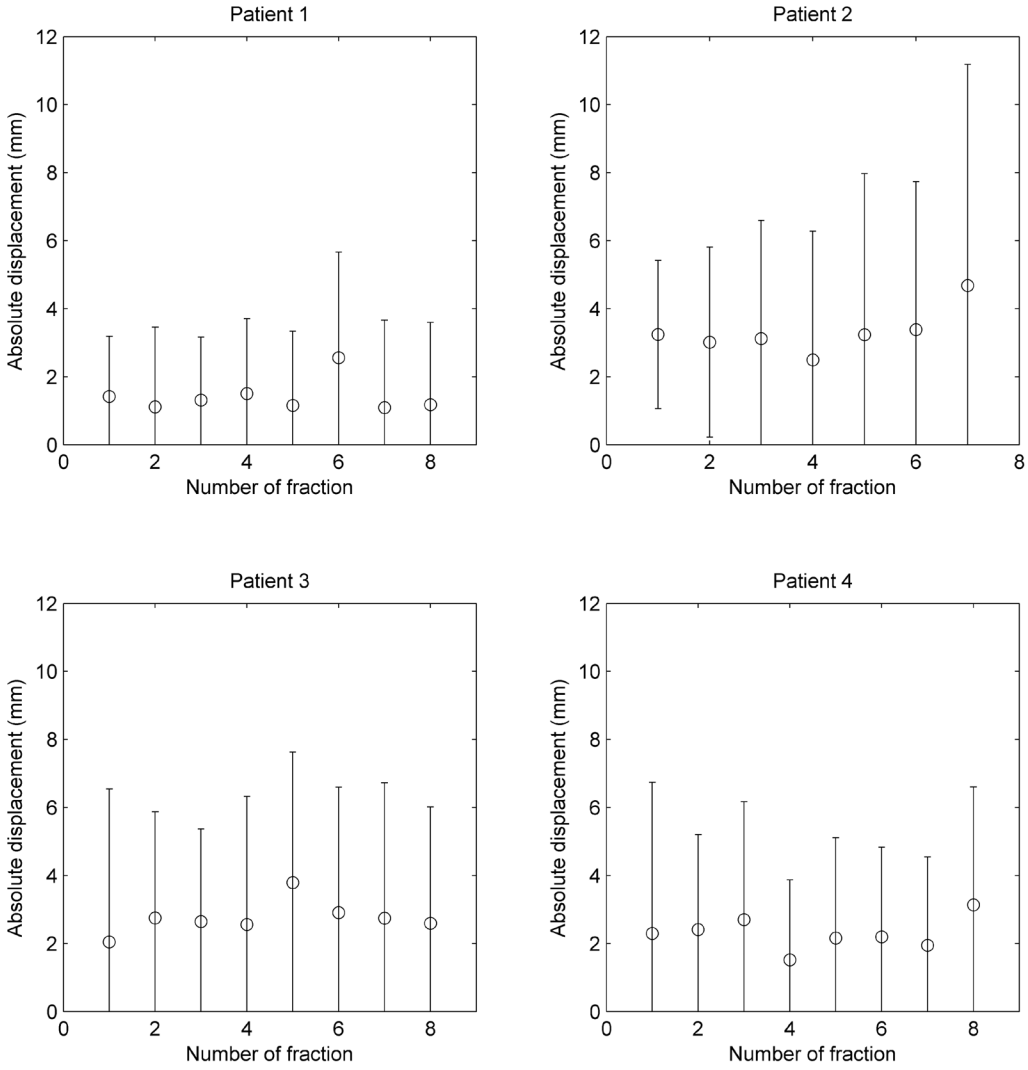


**Figure 2.**
Mean value of the absolute displacement for each fraction for the patients with weekly cine MV images. The error bars lengths correspond to two standard deviations.

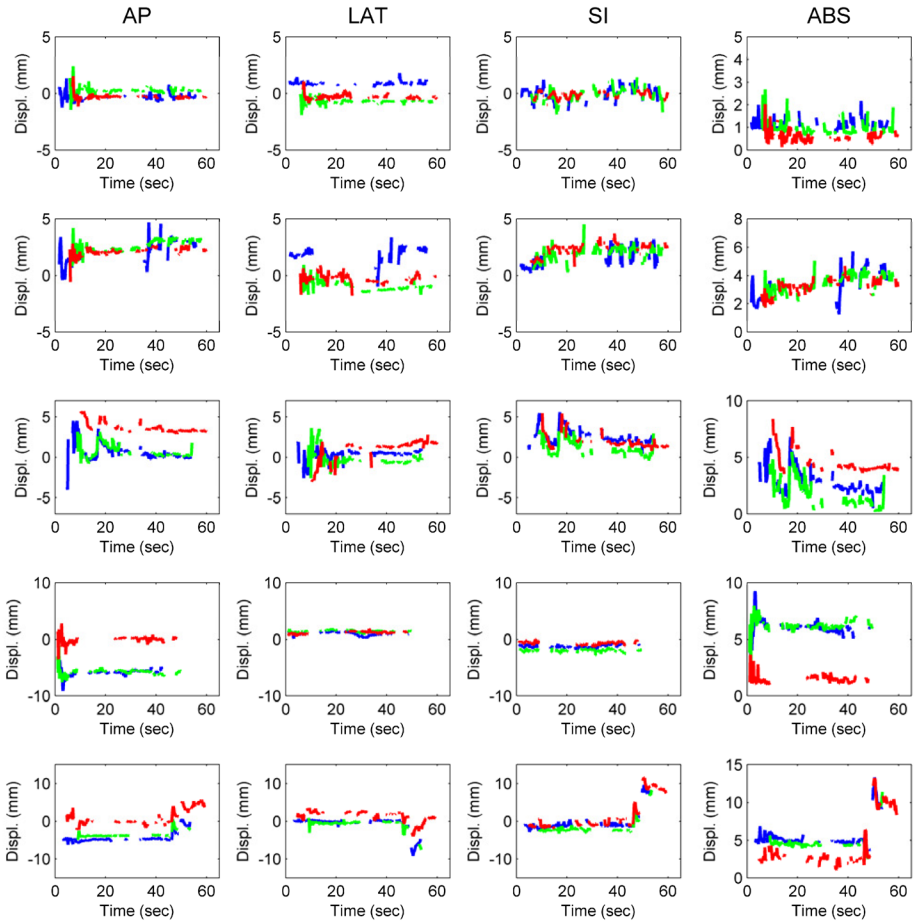


**Figure 3.**

Prostate motion trajectories identified with the cine MV system based on EPID. Each color corresponds to one of the three fiducials (blue: fiducial 1; green: fiducial 2; red: fiducial 3). Five arcs were examined for patient 1 (CW arc on fractions 5 and 6 depicted in rows 1 and 2), patient 2 (CCW arc for fractions 5 and 7 depicted on rows 3 and 5), and patient 7 (CW arc for first fraction depicted on row 4). In row 3 the AP and SI movements are clearly correlated.

**Table 1**

Percentages of detectability of the fiducials

| | | *Percentage* | | | |
|---|---|---|---|---|---|
| **Patient** | **Arc** | ***F1*** | ***F2*** | ***F3*** | ***At least one fiducial detectable*** |
| 1 | CW | 50.0 | 60.4 | 53.0 | 87.1 |
| | CCW | 44.1 | 27.1 | 34.3 | 62.8 |
| 2 | CW | 20.9 | 24.5 | 31.5 | 49.0 |
| | CCW | 65.4 | 61.3 | 66.6 | 90.2 |
| 3 | CW | 41.0 | 25.2 | 40.4 | 60.7 |
| | CCW | 3.2 | 7.9 | 0.1 | 10.9 |
| 4 | CW | 27.5 | 12.8 | 17.0 | 28.6 |
| | CCW | 16.8 | 26.7 | 26.6 | 35.6 |
| 5 | CW | 77.1 | 27.1 | 28.0 | 85.4 |
| | CCW | 4.9 | 29.3 | 24.8 | 41.7 |
| 6 | CW | 58.7 | 70.0 | 20.8 | 82.4 |
| | CCW | 0.0 | 0.0 | 13.7 | 13.7 |
| 7 | CW | 56.9 | 50.6 | 51.0 | 65.5 |
| | CCW | 26.4 | 19.2 | 26.4 | 44.9 |
| 8 | CW | 49.7 | 63.4 | 44.9 | 94.5 |
| | CCW | 36.1 | 31.0 | 51.9 | 71.7 |
| 9 | CW | 36.4 | 28.9 | 29.8 | 39.9 |
| | CCW | 41.6 | 49.4 | 46.9 | 64.3 |
| 10 | CW | 34.9 | 54.6 | 66.2 | 77.5 |
| | CCW | 33.4 | 8.7 | 3.7 | 24.4 |

CW: clockwise; CCW: counterclockwise; F1 – F3: fiducials 1 – 3.

**Table 2**

Summary of the motion assessment in prostate patients

| | *Mean (mm)* | | | | *Standard deviation σ (mm)* | | | | |
|---|---|---|---|---|---|---|---|---|---|
| **Patient number** | **AP** | **LAT** | **SI** | **ABS** | **AP** | **LAT** | **SI** | **ABS** | **Number fractions** |
| 1 | 0.70 | 0.76 | 0.70 | 1.42 | 0.81 | 0.91 | 0.73 | 1.25 | 8 |
| 2 | 2.22 | 1.28 | 1.45 | 3.32 | 1.78 | 1.51 | 1.27 | 2.18 | 7 |
| 3 | 2.05 | 1.23 | 1.07 | 2.93 | 2.00 | 1.54 | 0.90 | 2.34 | 8 |
| 4 | 1.50 | 1.02 | 0.97 | 2.32 | 1.35 | 1.24 | 0.78 | 1.68 | 8 |
| 5 | 1.51 | 0.80 | 1.62 | 2.61 | 1.28 | 0.84 | 1.26 | 1.63 | 4 |
| 6 | 2.21 | 1.51 | 1.93 | 3.61 | 1.72 | 1.28 | 1.26 | 2.02 | 2 |
| 7 | 2.31 | 1.40 | 0.94 | 3.25 | 2.30 | 1.33 | 0.66 | 2.26 | 2 |
| 8 | 1.20 | 0.72 | 0.83 | 1.86 | 1.10 | 1.10 | 0.80 | 1.50 | 2 |
| 9 | 1.15 | 0.97 | 0.96 | 1.40 | 1.02 | 0.97 | 0.69 | 1.29 | 1 |
| 10 | 1.58 | 1.64 | 2.38 | 3.68 | 1.77 | 1.39 | 1.20 | 1.95 | 1 |

*Int J Radiat Oncol Biol Phys*. Author manuscript; available in PMC 2014 July 15.

**Table 3**

Percentage of tracked time in which the displacement is larger than a predefined threshold

| | % time with Δ > 3 mm | | | % time with Δ > 5 mm | | |
|---|---|---|---|---|---|---|
| **Patient** | **AP** | **LAT** | **SI** | **AP** | **LAT** | **SI** |
| 1 | 2.8 | 1.8 | 1.7 | 0.3 | 0.8 | 0.0 |
| 2 | 32.1 | 6.9 | 7.8 | 3.8 | 2.1 | 1.8 |
| 3 | 14.1 | 5.7 | 4.1 | 6.0 | 2.6 | 0.3 |
| 4 | 10.7 | 7.9 | 2.0 | 2.9 | 1.7 | 0.0 |
| 5 | 6.8 | 2.8 | 11.3 | 1.2 | 0.5 | 3.2 |
| 6 | 24.8 | 8.1 | 21.2 | 9.8 | 2.1 | 1.8 |
| 7 | 28.0 | 6.1 | 0.5 | 24.1 | 2.1 | 0.0 |
| 8 | 3.1 | 1.4 | 2.0 | 0.9 | 0.7 | 0.5 |
| 9 | 3.4 | 2.3 | 0.1 | 1.4 | 0.5 | 0.0 |
| 10 | 6.8 | 10.2 | 30.5 | 2.3 | 5.3 | 1.4 |

*Int J Radiat Oncol Biol Phys*. Author manuscript; available in PMC 2014 July 15.